Available online at www.sciencedirect.com

ScienceDirect

Advances in Space Research 63 (2019) 63–72

ADVANCES IN SPACE RESEARCH (a COSPAR publication)

www.elsevier.com/locate/asr

Time-varying solar radiation pressure on Ajisai in comparison with LAGEOS satellites

Akihisa Hattori [a,*], Toshimichi Otsubo [b]

[a] Department of Polar Science, SOKENDAI (The Graduate University for Advanced Studies), Tokyo, Japan
[b] Hitotsubashi University, Tokyo, Japan

Received 31 May 2018; received in revised form 26 July 2018; accepted 7 August 2018
Available online 14 August 2018

Abstract

This study aims to investigate solar radiation pressure acting on the spherical geodetic satellites, Ajisai, LAGEOS-1, and LAGEOS-2. The solar radiation pressure coefficients (C_R) are derived in two independent ways: (a) through precise orbit determination (POD) using satellite laser ranging (SLR) data, and (b) through modeling using the optical properties of the satellite surface material. The average C_R value of Ajisai (1.039), as calculated from the time series of C_R POD estimates every 15 days, is consistently smaller than those of LAGEOS-1 (1.140) and LAGEOS-2 (1.103). This difference can be explained by the fact that the surface of Ajisai is mostly covered by mirrors. The Ajisai C_R values estimated by POD show remarkable semi-annual variation, which disagrees with the results of a previous study (Sengoku et al., 1995) predicting that the C_R of Ajisai varies almost annually. We attribute this semi-annual variation to two physical reasons: the non-spherical additional cross-sectional area due to the "attached fitting ring" and the low reflectivity of the surface material in the polar regions. Furthermore, the solar radiation pressure acting on Ajisai varies annually in a direction perpendicular to the sun-satellite vector. Finally, the two independent C_R values of Ajisai agree more when we assume a total solar irradiance of 1361 W/m^2, whereas the value 1367 W/m^2 has been commonly used in POD.

Keywords: Orbit determination; Satellite laser ranging; Ajisai; LAGEOS

1. Introduction

Geodetic observations have been indispensable to understand the Earth system. In particular, global geodetic networks now provide a continuous and accurate monitoring of global-scale geodetic parameters such as terrestrial reference frames and earth gravity fields. Any systematic error source should be eliminated to provide consistent geodetic products. Precise orbit determination (POD) of artificial satellites plays a key role in global-scale geodesy. Various acceleration sources have been taken into consideration to describe the motion of artificial satellites which are being precisely observed by modern space geodetic techniques. Although gravitational forces dominate satellite dynamics, small perturbation forces such as solar radiation pressure have to be modeled as well in numerical orbit integration (Milani et al., 1987).

The force due to solar radiation pressure is caused by the momentum of photons radiated from the Sun, which are reflected or absorbed at the surface of the satellite, and the acceleration is the force divided by the mass (m) of the satellite. The acceleration is proportional to the cross-sectional area (A) of the satellite, and depends on the optical properties of the satellite surface material.

Solar radiation pressure is considered the largest error source in POD for global navigation satellite systems

* Corresponding author.
E-mail addresses: hattori_akihisa@anet.soken.ac.jp (A. Hattori), t.otsubo@r.hit-u.ac.jp (T. Otsubo).

https://doi.org/10.1016/j.asr.2018.08.010
0273-1177/

(GNSSs). For instance, Ziebart and Dare (2001) constructed an orientation-dependent solar radiation pressure model for GLONASS satellites with sunlight ray-tracing. It is also possible to construct or improve empirical models of solar radiation pressure acceleration (e.g. Sośnica et al., 2015b; Steigenberger et al., 2015; Montenbruck et al., 2017). In all of these studies, satellite laser ranging (SLR) data were proved suitable for investigating in detail the dynamics of satellites with complex shapes. This is because the radial components of their orbits can be accurately monitored as SLR directly measures the absolute distance between the station and the satellite.

The spherical geodetic satellites are focused in this paper. A spherically symmetric model (cannonball model) has been adopted for spherical geodetic satellites designed exclusively for SLR (McCarthy, 1996). Such a simplified model has been sufficient, because the actual cross-sectional area of such a satellite is independent of its orientation with respect to the Sun and the satellite structure is almost spherically symmetrical. The only equivocal exception is a study conducted by Sengoku et al. (1995) on Ajisai. They demonstrated that an asymmetric model improved the orbit determination of the satellite as described in Section 2. Scharroo et al. (1991) suggested that the LAGEOS-1 (LAser GEOdynamics Satellite 1) along-track acceleration may be explained by assuming an inequality in the matte finish, i.e. the roughness of the aluminum surface, causing the asymetry of/in sunlight reflectivity, between the two hemispheres of LAGEOS-1.

Ajisai has been the most observed satellite from the worldwide SLR stations, in terms of the number of passes. SLR data to Ajisai have been used for earth gravity field determination (Matsuo et al., 2013; Sośnica et al., 2015a), experimentally for terrestrial reference frames (Sośnica et al., 2014) and for spin-parameter determination (Otsubo et al., 2000; Kucharski et al., 2010).

As summarized in Table 1, in comparison with other satellites including the two LAGEOS (0.60 m), Ajisai has a larger diameter (2.15 m). The mass of Ajisai is 685 kg, which is slightly less than double of the LAGEOS satellites (Fitzmaurice et al., 1977; Minott et al., 1993; Sasaki and Hashimoto, 1987). The A/m ratio of Ajisai is close to eight times larger than those of the LAGEOS satellites, and therefore it is more sensitive to solar radiation pressure.

In this paper, precise orbit analysis of Ajisai and the LAGEOS satellites are firstly, in Section 2, conducted to investigate the time-varying solar radiation pressure, and the optical properties of satellite surface material are secondly used to construct a solar radiation pressure model in Section 3. These two independent outcomes are compared and discussed in Section 4, and the paper is concluded in Section 5.

Table 1
Mission parameters of Ajisai, LAGEOS-1, and LAGEOS-2.

	Ajisai	LAGEOS-1	LAGEOS-2
Launch date	Aug. 12, 1986	May 4, 1976	Oct. 22, 1992
Diameter [m]	2.15	0.60	0.60
Mass [kg]	685	406.965	405.38
A/m [m^2/kg]	0.0053	0.00069	0.00070
Altitude [km]	1,490	5,860	5,620
Inclination [degree]	50.0	109.84	52.64

2. Solar radiation pressure acceleration model and orbit determination

2.1. Cannonball model for solar radiation pressure

A cannonball model is being adopted in the orbit generation and determination of the spherical geodetic satellites. This model is based on the simplified assumptions that the satellite is fully-spherical and the optical properties of its surface material are uniform.

In this model, the acceleration of solar radiation pressure $\ddot{\boldsymbol{r}}$ is given as:

$$\ddot{\boldsymbol{r}} = \mu \frac{I}{c} C_R \left(\frac{AU}{|\boldsymbol{R}|}\right)^2 \frac{A}{m} \frac{\boldsymbol{R}}{|\boldsymbol{R}|} \tag{1}$$

where μ is the portion of the Sun's cross-sectional area seen from a satellite (0 in shadow and 1 in sunlight); I is total solar irradiance (TSI), where 1367 W/m^2 is widely used; c is the speed of light; AU is an astronomical unit; $\boldsymbol{R}$ is the vector from the Sun to the satellite; A is the cross-sectional area of the satellite seen from the Sun's direction; and m is the mass of the satellite. C_R is a solar radiation pressure coefficient, which is often treated as an adjusting parameter in orbit determination and is defined by how the surface of the satellite reflects or absorbs photons.

For example, assuming that C_R is 1.0, μ is 1 and a satellite is at 1 AU distance from the Sun, the solar radiation pressure acceleration amounts to 2.42×10^{-8} m/s^2 for Ajisai and 3.18×10^{-9} m/s^2 for LAGEOS.

Sengoku et al. (1995) predicted an annual cyclic pattern of solar radiation pressure acting on Ajisai. They also introduced an acceleration model for axially symmetric but spherically asymmetric satellites. In addition to Eq. (1), they extended the solar radiation pressure acceleration to the direction that is perpendicular to the sun-satellite direction and lies within a plane containing both the sun-satellite direction and symmetry axis $\hat{\boldsymbol{s}}$. The correction term was formulated with an additional adjusting parameter C_{AR} as:

$$\ddot{\boldsymbol{r}}_t = \mu \frac{I}{c} C_{AR} \left(\frac{AU}{|\boldsymbol{R}|}\right)^2 \frac{A}{m} \hat{\boldsymbol{t}} \tag{2}$$

where

$$\hat{\boldsymbol{t}} = -\frac{\boldsymbol{R} \times \hat{\boldsymbol{s}}}{|\boldsymbol{R} \times \hat{\boldsymbol{s}}|} \times \frac{\boldsymbol{R}}{|\boldsymbol{R}|} \tag{3}$$

This model was formulated for general purposes but has been applied only to the Ajisai satellite so far.

2.2. Orbit determination

In this section, a time-series of solar radiation coefficients, C_R^{POD} and C_{AR}^{POD}, are derived from POD.

We estimate the solar radiation pressure coefficients of Ajisai, LAGEOS-1 and LAGEOS-2 by POD using the space geodetic analysis software "c5++." We use SLR observation data (Pearlman et al., 2002; Noll, 2010) from the three satellites obtained by 37 ILRS stations between 1993 and 2016, which are separated into many 15-day spans. The physical models and analysis conditions are summarized in Table 2.

We estimate the range bias to absorb the station-dependent constant offset errors (Appleby et al., 2016) and treat it as a common parameter for LAGEOS-1 and LAGEOS-2 and a separate parameter for Ajisai because of the different target-signature effects (Otsubo and Appleby, 2003). We do not estimate once-per-revolution acceleration parameters, because they are highly correlated with solar radiation pressure coefficients and earth gravity field coefficients (Sośnica et al., 2012).

2.3. Time-varying coefficients of C_R^{POD} and C_{AR}^{POD}

After applying orbit determination, the root mean square (RMS) of the post-fit residuals are 1–2 cm for LAGEOS-1 and LAGEOS-2, and 2–4 cm for Ajisai.

We obtain the solar radiation pressure coefficients (C_R^{POD} for LAGEOS-1, LAGEOS-2 and Ajisai, and C_{AR}^{POD} for Ajisai) every 15 days and the time series are plotted in Fig. 1.

The average (and RMS followed by $\pm$) of the coefficient C_R^{POD} after 2000 are 1.140 ± 0.014 for LAGEOS-1, 1.103 ± 0.012 for LAGEOS-2, 1.039 ± 0.008 for Ajisai, and those of C_{AR}^{POD} are 0.006 ± 0.015 for Ajisai. The C_R^{POD} solutions for Ajisai are more stable than those for the two LAGEOS satellites. This is because Ajisai is more perturbed by solar radiation pressure due to the higher A/m ratio. We observe that the C_R^{POD} of Ajisai is significantly smaller than those of the two LAGEOS satellites, which is discussed in Section 4. We also observe interesting features in the LAGEOS-1 and LAGEOS-2 solutions; the C_R^{POD} estimates for LAGEOS-1 are slightly but constantly higher by 0.037 than those for LAGEOS-2. The LAGEOS-1 time-series scatters more due to unknown reasons, and the LAGEOS-2 time series show systematic trends in the 1990s. Therefore, we remove the solutions for the 1990s in the above computations of the average value and RMS of C_R^{POD}.

By magnifying the time scale on the abscissa of Fig. 1, a repeating pattern is clearly detected in C_R^{POD} and C_{AR}^{POD} of Ajisai. The four graphs in Fig. 2 are based on the same dataset as Fig. 1 but plotted with respect to a day of year so that a seasonal signal is easily seen. We observe no periodic patterns in C_R^{POD} of LAGEOS-1 and LAGEOS-2, but clear seasonal patterns in C_R^{POD} and C_{AR}^{POD} of Ajisai.

3. Optical reflection model by a ray-tracing method

3.1. Physical mechanism of solar radiation pressure

The behavior of photons at the surface of a satellite determines the magnitude and direction of the solar radiation pressure. The surfaces of the three satellites studied in this paper consist of aluminum and corner cube reflectors (CCR). In addition, Ajisai is also covered by mirrors and glass fiber reinforced plastic (GFRP).

Table 2
Physical models and analysis conditions in orbit determination.

Component	model/condition
Software	
c5++	version 898
Models	
Station coordinates	ITRF2014 (Altamimi et al., 2016)
Satellites	Ajisai, LAGEOS-1 and LAGEOS-2
Earth gravity	EGM2008 (Pavlis et al., 2012)
Atmospheric density model	DTM-2013 (Bruinsma, 2015)
Planetary ephemeris	JPL DE423 (Folkner, 2010)
Earth orientation parameter	EOP 14 C04 (IAU2000A)
Others	IERS Conventions (Petit and Luzum, 2010)
Solved-for parameters	
Satellite position and velocity	per satellite and per 5 days
C_R	per satellite and per 15 days
C_{AR}	per 15 days for Ajisai
Atmospheric drag coefficient	per 5 days for Ajisai
Empirical along-track acceleration	per 5 days for LAGEOS-1 and LAGEOS-2
Range bias	per station and per 15 days, a common parameter for LAGEOS-1 and LAGEOS-2, and a separate parameter for Ajisai
Geocenter	per 15 days
Earth gravity coefficients	per 15 days, up to degree/order 4

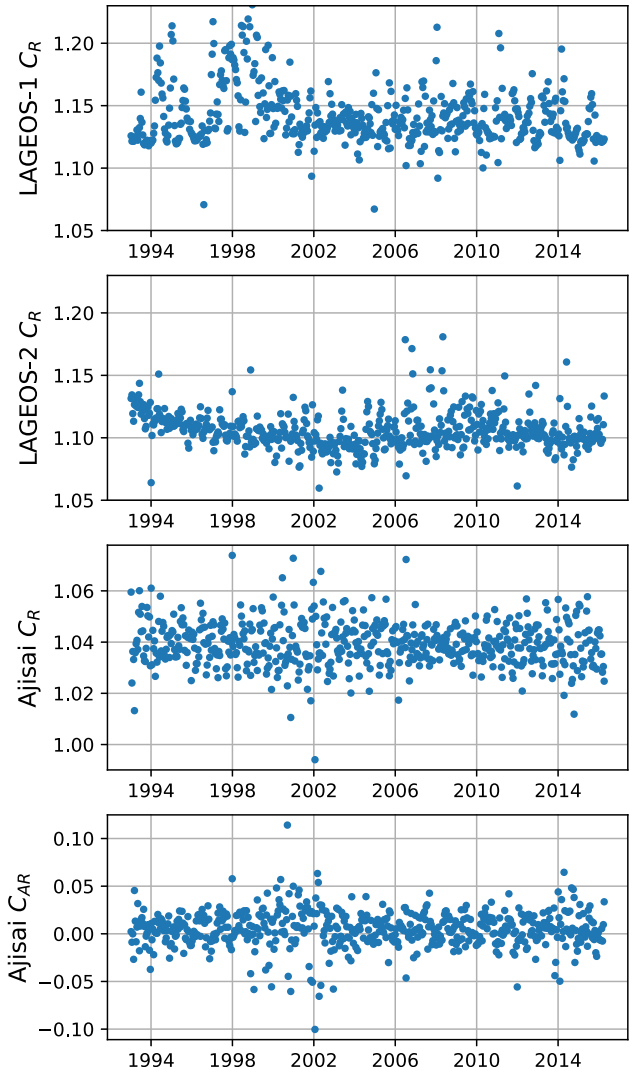

Fig. 1. Estimated solar radiation coefficients of LAGEOS-1, LAGEOS-2 and Ajisai.

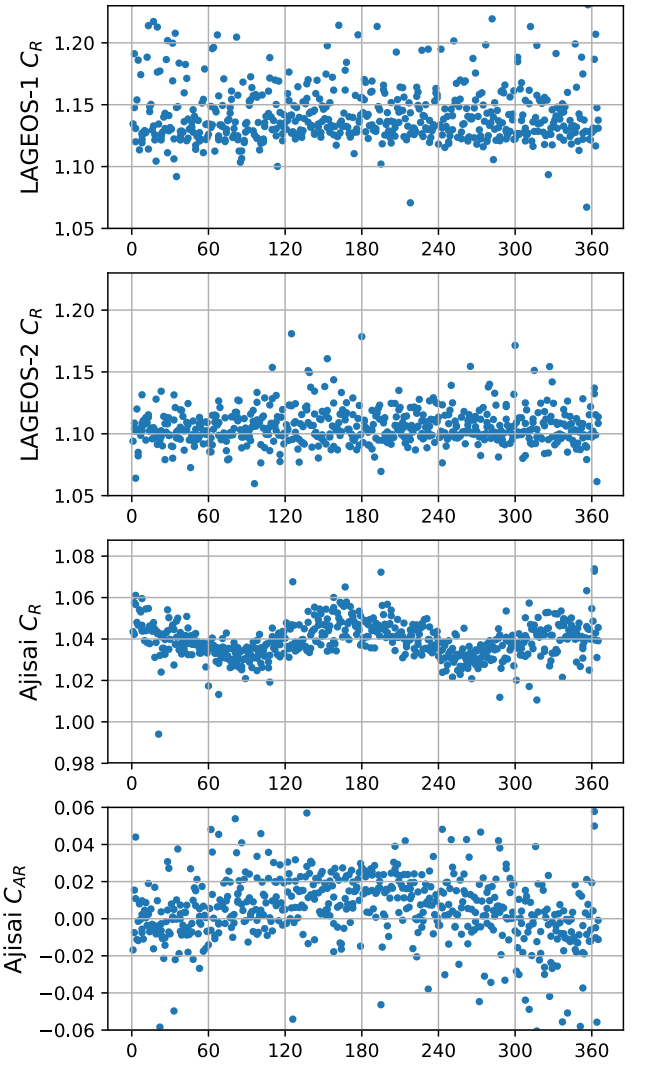

Fig. 2. Estimated solar radiation coefficients of LAGEOS-1, LAGEOS-2 and Ajisai, aligned by a day of year.

Following a model formulated based on in Sengoku et al. (1995), we also define the three factors affecting optical interactions at the surface of the satellites: specular (subscript s hereafter), diffuse (d) and backward reflection (b) (Fig. 3).

Specular reflection occurs at any material but it is maximized at specular material like the mirrors on Ajisai. On the contrary, in diffuse reflection, photons are emitted isotropically. Among the surface material on the satellites, this occurs largely at GFRP and aluminum. In backward reflection that is specific to CCRs on spherical geodetic satellites, the outgoing photons travel toward the reverse direction of the incoming photons.

Given the optical reflection properties and satellite dimensions, independent of the orbit determination, the force acting on the satellite per unit radiation pressure $\boldsymbol{F}_r$ is expressed by the following surface integral:

$$\boldsymbol{F}_r = A\hat{\boldsymbol{e}}_b + \iint_{\sigma}\left(r_s f_s \hat{\boldsymbol{e}}_s + \frac{2}{3} r_d f_d \hat{\boldsymbol{e}}_d + r_b f_b \hat{\boldsymbol{e}}_b\right) g\cos\theta d\sigma \quad (4)$$

where A is the cross-sectional area of the satellite, r is the reflectivity, f is the ratio of an optical reflection type ($f_s + f_d + f_b = 1$), $\hat{\boldsymbol{e}}$ is the unit vector defined in the upper part of Fig. 3, σ is a surface element, g is 1 when σ is illuminated by incident light and is 0 when not, and θ is the angle of incidence toward σ.

Then, the solar radiation coefficients C_R and C_{AR} are expressed by the following inner product of $\boldsymbol{F}_r$ and each directional vector ($C_R^{Material}$ and $C_{AR}^{Material}$):

$$C_R^{Material} = \frac{\boldsymbol{F}_r}{A} \cdot \frac{\boldsymbol{R}}{|\boldsymbol{R}|} \quad (5)$$

$$C_{AR}^{Material} = \frac{\boldsymbol{F}_r}{A} \cdot \hat{\boldsymbol{t}} \quad (6)$$

In the extreme case of a sphere covered by a perfect mirror, the $C_R^{Material}$ would be exactly 1. In another extreme case that a satellite consist of a single ideal circular-face CCR and it faces the Sun, the $C_R^{Material}$ would be exactly 2.

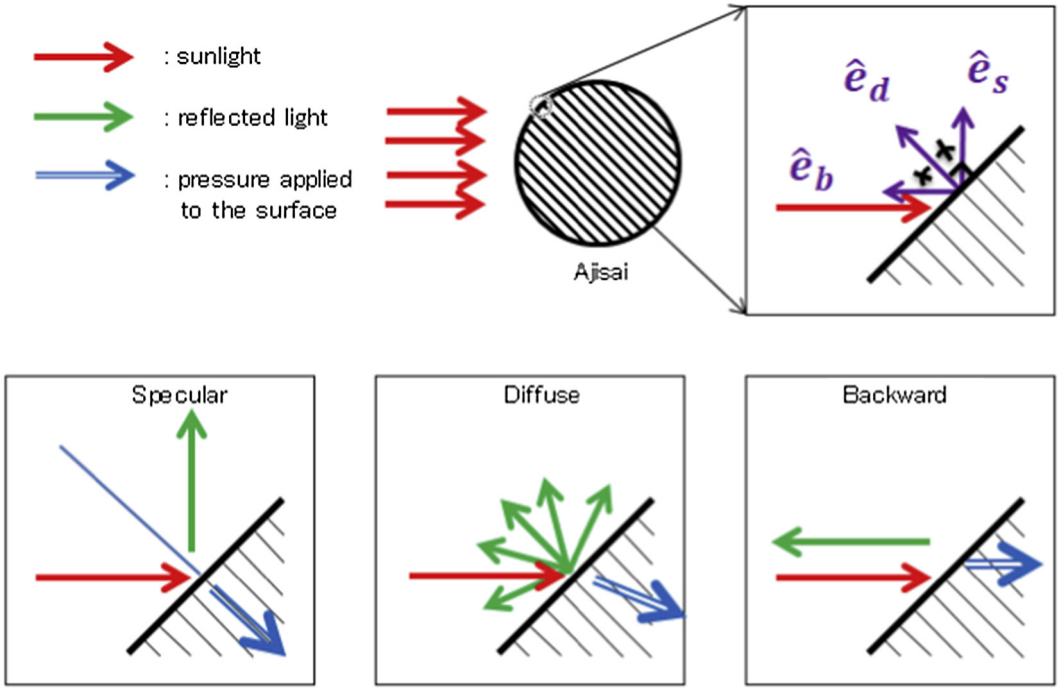

Fig. 3. Schematic diagrams of the three reflection types modeled in Eq. (4). The blue arrows indicate the direction of acceleration, which depend on the incident surface material. $\hat{e}_b$ is a direction vector in the direction opposite to the incident light, $\hat{e}_d$ is a direction vector perpendicular to the satellite surface and $\hat{e}_s$ is a direction vector of specular reflection. (For interpretation of the references to color in this figure legend, the reader is referred to the web version of this article.)

We use a ray-tracing method to calculate the $C_R^{Material}$ value from Eq. (5). The ray-tracing method was initially developed for computer graphics to simulate the behavior of individual photons for irradiated objects modeled as a group of polygons and light as pixel-array. Several studies have proven that the precision of orbit determination of GNSS satellites is improved when modeling the solar radiation pressure with this method (Ziebart and Dare, 2001; Tan et al., 2016). Ray-tracing has the advantage that the resolution of the acceleration model can be easily enhanced with more polygons and a more dense pixel-array, although the computational cost increases.

To simulate the reflectance of aluminum, we use the values of the refractive index and extinction coefficient of aluminum in Haynes (2014). It should be noted that these values strongly depend on the surface finish, knowledge of which is not available for the three satellites. Therefore, the reflectance of the satellite's aluminum is only a rough approximation in this case.

Not all photons that hit the front surface of CCR are reflected backward, because the effective reflection area is smaller than the full front surface area and some photons are reflected specularly at the surface without entering the CCR prism. The effective reflection area and the reflectance of CCR are based on the functions of Otsubo and Appleby (2003, Fig. 3 and 4).

The mirrors on Ajisai are considered as fully specular material. The reflectance of GFRP on Ajisai is taken from Hashimoto (2018), although only 7% of the Ajisai surface is occupied by GFRP and its contribution to $C_R^{Material}$ is marginal.

3.2. Surfaces of LAGEOS and Ajisai

The spherical bodies of the LAGEOS satellites are made of aluminum, and 426 CCRs are mounted on each satellite. The CCRs are almost uniformly distributed on the surface and their optical properties are considered those of spherically symmetrical objects. Overall, 57% of the satellite's surfaces is covered by aluminum and 43% is covered by CCRs (Fitzmaurice et al., 1977; Minott et al., 1993).

On the contrary, Ajisai has a more complex form (Sasaki and Hashimoto, 1987). The diameter of Ajisai is 2.15 m. Most of the surface is covered by 318 mirrors and 120 laser reflector assemblies. The mirrors are designed for sunlight reflection and the largest size of each mirror is 20 × 20 cm. Each laser reflector assembly consists of an aluminum-made container and 12 CCRs for SLR. In total, 78.0% of the surface is covered by mirrors, 7.5% by aluminum, 7.1% by CCRs, and 7.0% by GFRP.

The surface of Ajisai deviates more from spherical symmetry than LAGEOS satellites in two ways. First, the mirrors and laser reflector assemblies are arranged in 15 cylindrical rows centered around the rotation axis of Ajisai, and each row has a different composition of mirrors and laser reflector assemblies. The central 13 rows are nearly uniform, but the polar rows are not because the GFRP is partly exposed. Second, the shape of Ajisai is not a simple

sphere due to a small aluminum part, the attached fitting ring (radius = 48 cm and height = 5 cm), being attached to one of the poles. It was used to hold the satellite body to the H-l rocket at launch and spin the satellite at the time of release. Such a structure is not present in other spherical geodetic satellites. This additional part was described in Sasaki and Hashimoto (1987), but there have not been any studies that take the asymmetry caused by this attachment into account.

To examine how the difference in the surfaces of the satellites impacts the solar radiation pressure, we design a 3D model based on the actual layout of the surface materials and their optical properties (Fig. 4) to quantify the influence of the nonuniformity of the surface.

3.3. $C_R^{Material}$ from the 3D model

As mentioned above, the characteristic of reflections on aluminum is dependent on the finish of the surface. However, the only description of the satellite's aluminum that we have found is "diffuse aluminum" in Siry (1975); details were not given in the prelaunch articles on LAGEOS and Ajisai (Fitzmaurice et al., 1977; Minott et al., 1993; Sasaki and Hashimoto, 1987). Therefore, we assume a large range of the diffuse reflection ratio ($r_d/(r_d + r_s)$) from 0.2 to 0.95, and we take 0.6 as a representative value.

As a result of the numerical integration of Eq. (5), the $C_R^{Material}$ of LAGEOS is derived in the range from 1.081 to 1.253.

While we use estimates for all incidence angles for the LAGEOS satellites, we cannot do the same for Ajisai because of the asymmetry. The angle between the Earth's rotation axis and the direction of the Sun is 90±23.4°. The spin axis of Ajisai is almost parallel to the Earth rotation axis (Sasaki and Hashimoto, 1987; Kucharski et al., 2010). The angle of incidence is limited to ±23.4° around the equator, when the two axes are assumed exactly parallel.

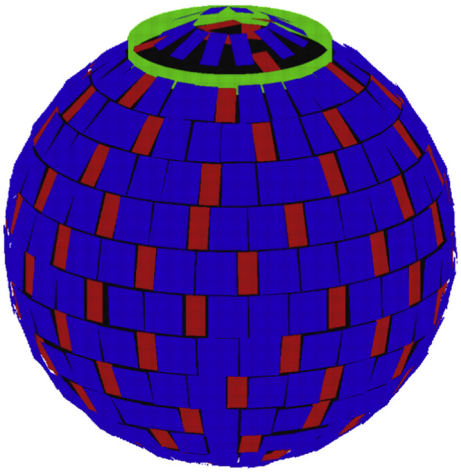

Fig. 4. The surface of Ajisai. Mirrors are drawn in blue, laser reflector assemblies in red, the attached fitting ring in green and GFRP in black. (For interpretation of the references to color in this figure legend, the reader is referred to the web version of this article.)

Sengoku et al. (1995) simplified the asymmetry by dividing the surface of Ajisai into three regions: south polar cap, main body, and north polar cap. In each region, the parameters for optical properties were assumed uniform. We take into account all of the major parts such as mirrors, aluminum, corner cube prisms, and GFRP, and we input them into Eqs. (5) and (6). Our model is based on 441 parts, and therefore we expect our model is more precise.

Indeed, the mirrors on Ajisai are less populated in the polar regions than that at the low and middle latitude regions. The two polar regions are not symmetric. The mirrors on the north polar region are even less populated than those on the south polar region. Instead, the GFRP that reflects diffusely is more exposed in the north polar region. In summer, less specular, more diffuse components are slantingly illuminated by the Sun, which results in an increase of C_R.

Sengoku et al. (1995), therefore, modeled the seasonal variation of C_R. The annual component was dominant while the semi-annual component was also observed. Based on their results, the magnitude of the annual component of C_R is 0.0068, and that of the semi-annual component is 0.0025.

In Sengoku et al. (1995), the mirrors are attached on its surface, implying that the radius of their curvature is equal to the radius of the spherical body. However, our model is based on a flat mirror, which is considered a good approximation to the reality (8.5 to 9 m of the curvature radius). The surface behaves less specularly where the angle of sunlight-incidence is large and the coefficient C_R is larger than Sengoku et al. (1995) by 0.003–0.009.

We also find that the additional cross-sectional area due to the attached fitting ring is not negligible and varies with time. Fig. 5 shows how Ajisai is seen from the Sun during each season. The attached fitting ring is attached around the lower pole which nearly directs the north. In the spring and autumn, the angle between the equator and the direction of the Sun is small, and therefore the additional cross-sectional area, due to the attached fitting ring, is minimized. In the summer and winter, however, the cross-sectional area becomes maximum because the attached fitting ring is slantingly illuminated.

The left graph in Fig. 6 shows the ratio of the increased cross-sectional area due to the attached fitting ring with respect to the angle of incidence from the equator. The angle of incidence remains almost constant within ±23.4°. The increased ratio is symmetrical around the equator. The minimum value is 0.0012% at zero degrees latitude, and the maximum value is 0.0099% at 21° latitude. The right graph in Fig. 6 shows the same ratio with respect to a day of year. It is clear that the semi-annual component dominates and it is maximized in summer and winter.

To incorporate the time-varying cross-sectional area (A), we rewrite Eq. (1) as:

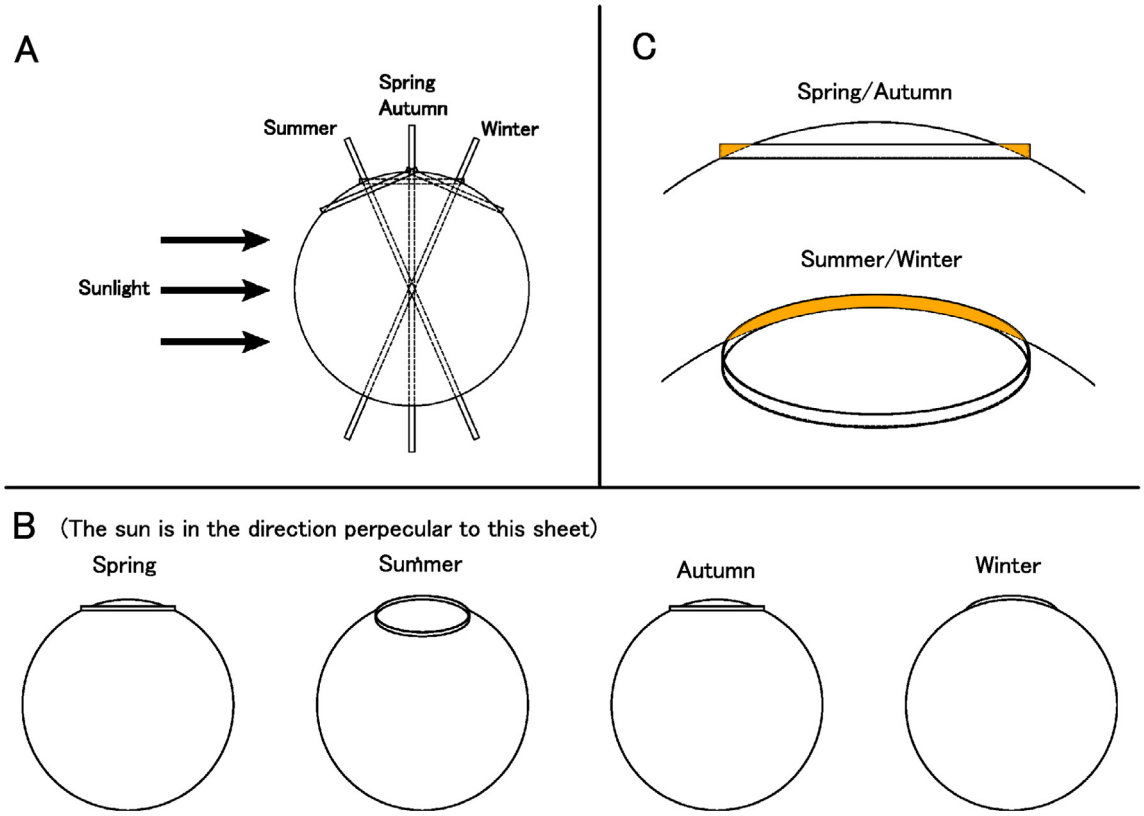

Fig. 5. The geometry of the attached fitting ring of Ajisai. The drawings at the bottom are simply magnified from the ones at the top. A and B: Seasonal variation of the sun-satellite geometry, seen from different directions. C: Magnified drawings around the additional cross-sectional area (in orange). (For interpretation of the references to color in this figure legend, the reader is referred to the web version of this article.)

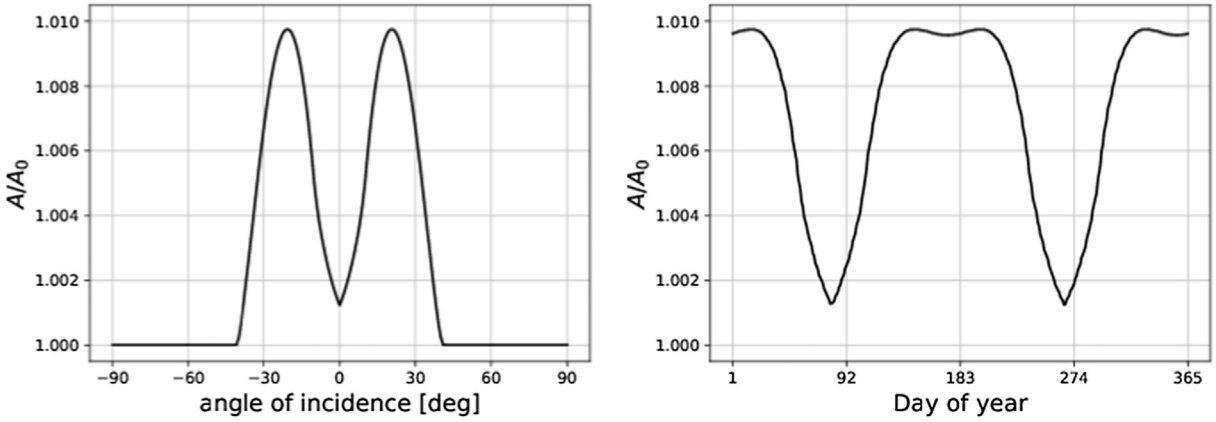

Fig. 6. The variation of the cross-sectional area of Ajisai with respect to the angle of incidence throughout the year.

$$\ddot{\boldsymbol{r}} = \mu \frac{I}{c} C_R \left(\frac{AU}{|\boldsymbol{R}|}\right)^2 \frac{A}{m} \frac{\boldsymbol{R}}{|\boldsymbol{R}|} \tag{7}$$

$$= \mu \frac{I}{c} \left(\frac{A}{A_0} C_R\right) \left(\frac{AU}{|\boldsymbol{R}|}\right)^2 \frac{A_0}{m} \frac{\boldsymbol{R}}{|\boldsymbol{R}|} \tag{8}$$

where A_0 is the reference cross-sectional area (3.631 m^2 for Ajisai). The derived annual average $(A/A_0)C_R^{Material}$ of Ajisai falls in the range from 1.034 to 1.070.

4. Comparison and discussion

Considering the C_R values of Ajisai, LAGEOS-1, and LAGEOS-2 that are estimated by POD (Section 2) and those independently derived from the satellites surfaces' optical properties (Section 3), the variation in the cross-sectional area is not negligible only in the case of Ajisai. However, the cross-sectional area of Ajisai is fixed to 3.631 m^2 in the orbit determination procedure. The estimated

C_R^{POD} values are subject to vary because A varies in time. In this section, the factor A/A_0 is thus multiplied to C_R.

Both values are in good agreement with each other, as shown in Fig. 7. In each block of Ajisai and LAGEOS, the leftmost point with a bar shows the range of $C_R^{Material}$ described in Section 3. The points next to it are the average and the standard deviation of C_R^{POD} estimation described in Section 2. The C_R^{POD} estimated for each satellite is in the range of $C_R^{Material}$. The uncertainty of the former is much larger than the latter especially in the LAGEOS satellites because they are largely covered by aluminum, whose optical properties are known less precisely. In addition, the C_R value of Ajisai is significantly smaller and close to 1.0 because its surface is mostly covered by mirrors.

The black points in Fig. 8 are the estimated C_R^{POD} values plotted with respect to day of year. The blue dashed line is what the previous model of Sengoku et al. (1995) predicted. The green dashed line is based on our $C_R^{Material}$ model.

While the annual frequency is dominant in Sengoku et al. (1995), the semi-annual frequency is also observed in our model. This semi-annual pattern is again found to be dominant in the orbit determination results. Our model is proven to describe the seasonal variation better, as shown in Fig. 8.

The all-year averages of Sengoku et al. (1995), our modeled value, and POD estimates are 1.025, 1.052 and 1.039, respectively. Our model $C_R^{Material}$ seems to be consistently higher than C_R^{POD}.

The solar radiation pressure acceleration is proportional to the TSI (I in Eq. (1)), where 1367 W/m^2 is conventionally used. However, a recent report supported a smaller value of I =1361 W/m^2 (Kopp and Lean, 2011) based on accurate measurements from the SORCE (SOlar Radiation and Climate Experiment) satellite. The difference in C_R using the conventional value 1367 W/m^2 versus the new value 1361 W/m^2 is about 0.46% in C_R.

Therefore, if we accept the new value as correct, the C_R^{POD} estimates in Section 2 are underestimated by that

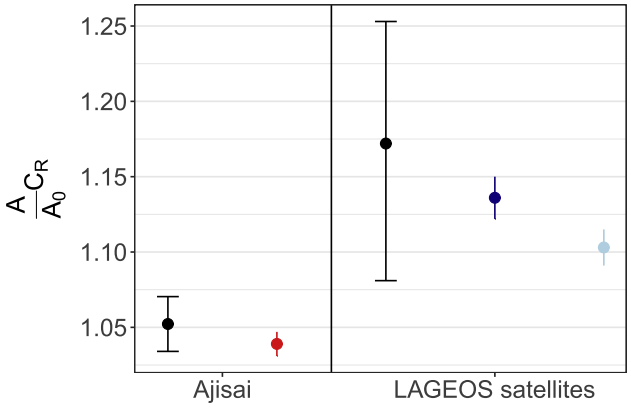

Fig. 7. Comparison of C_R^{POD} (red for Ajisai, dark blue for LAGEOS-1 and light blue for LAGEOS-2) and $C_R^{Material}$ (black) for Ajisai and LAGEOS. (For interpretation of the references to color in this figure legend, the reader is referred to the web version of this article.)

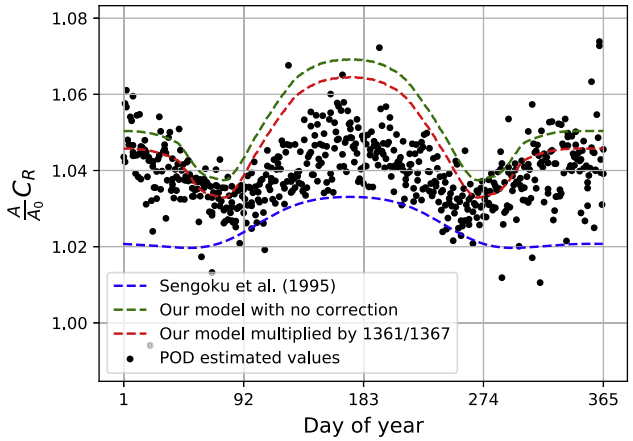

Fig. 8. C_R^{POD} estimates of Ajisai plotted with respect to day of year (black), and $C_R^{Material}$ curves from Sengoku et al. (1995) (blue), our model with no corrections (green) and our model with a correction of TSI (red). (For interpretation of the references to color in this figure legend, the reader is referred to the web version of this article.)

amount. Then, we plot the $C_R^{Material}$ in red by multiplying 1361/1367 with the green dashed curve. The all-year average of the red dashed line is 1.048, which becomes closer to the C_R^{POD} estimates. Therefore, our results indicate that the new value I =1361 W/m^2 fits better to the orbit determination result.

Even after applying the TSI adjustment, it is clear that our model estimate (red) deviates from the POD estimate (black) in summer. The semi-annual term is dominant in the POD estimates while the summer-winter difference is predicted by our model. The annual variation is caused by the difference between the optical properties in the two polar caps. Thus, the north-south asymmetry may be less significant in reality.

Let us look at the C_{AR} coefficient introduced in Eqs. (2) and (6). The annual patterns of $C_{AR}^{Material}$ produced by Sengoku et al. (1995) and our model are compared with the time series of the C_{AR}^{POD} estimates (Fig. 9). We see a clear annual-frequency signal in the POD estimates. The two models also ascertain the signal nicely. This is caused by the north-south asymmetry of the optical properties in the pole region. It should be noted that, in the discussion of C_{AR}, we do not have to take into account the increase in the cross-sectional area and the difference of TSI because C_{AR} is always close to zero.

At the end of this section, we present the seasonal variation of Ajisai C_R and C_{AR} predicted by our optical reflection model (red dashed curves in Figs. 8 and 9) as functions of doy (day of year):

$$\begin{aligned}\frac{A}{A_0}C_R^{Material} = {} & 1.0476 - 0.0099\cos\left(2\pi\tfrac{doy}{365}\right) + 0.0017\sin\left(2\pi\tfrac{doy}{365}\right) \\ & + 0.0096\cos\left(4\pi\tfrac{doy}{365}\right) - 0.0032\sin\left(4\pi\tfrac{doy}{365}\right) \\ & + 0.0009\cos\left(6\pi\tfrac{doy}{365}\right) - 0.0004\sin\left(6\pi\tfrac{doy}{365}\right) \\ & - 0.0024\cos\left(8\pi\tfrac{doy}{365}\right) + 0.0017\sin\left(8\pi\tfrac{doy}{365}\right)\end{aligned} \tag{9}$$

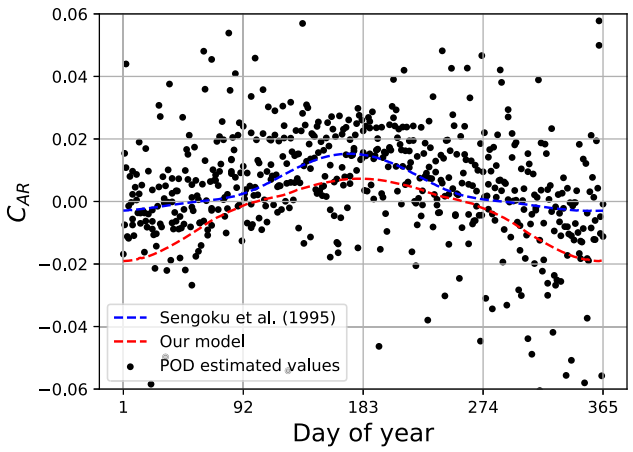

Fig. 9. C_{AR}^{POD} estimates of Ajisai plotted with respect to day of year (black), and $C_{AR}^{Material}$ curves from Sengoku et al. (1995) (blue) and our model (red). (For interpretation of the references to color in this figure legend, the reader is referred to the web version of this article.)

$$\frac{A}{A_0}C_{AR}^{Material} = 0.0041 - 0.0121\cos\left(2\pi\frac{doy}{365}\right) + 0.0026 \times \sin\left(2\pi\frac{doy}{365}\right) + 0.0018\cos\left(4\pi\frac{doy}{365}\right) - 0.0008\sin\left(4\pi\frac{doy}{365}\right) \quad (10)$$

We also present the empirical model based on our estimated values by POD (best-fit functions of black points in Figs. 8 and 9):

$$\frac{A}{A_0}C_{R}^{POD} = 1.0390 - 0.0010\cos\left(2\pi\frac{doy}{365}\right) + 0.0008 \times \sin\left(2\pi\frac{doy}{365}\right) + 0.0070\cos\left(4\pi\frac{doy}{365}\right) - 0.0019\sin\left(4\pi\frac{doy}{365}\right) \quad (11)$$

$$\frac{A}{A_0}C_{AR}^{POD} = 0.0054 - 0.0090\cos\left(2\pi\frac{doy}{365}\right) + 0.0022 \times \sin\left(2\pi\frac{doy}{365}\right) \quad (12)$$

These equations assume that the A_0 is fixed at 3.631 m^2 and I at 1367 W/m^2. When $I = 1361$ W/m^2 is adopted, the coefficients should be multiplied by 1367/1361.

5. Conclusions

Solar radiation pressure coefficients C_R are derived for Ajisai and the LAGEOS satellites in two ways: a POD time series and an optical reflection model. First, the C_R values of Ajisai are significantly smaller than those of the two LAGEOS satellites derived by either approach. This results from the difference in the surface properties and materials: most of the surface of Ajisai are covered by mirrors, but the surfaces of the LAGEOS satellites are composed of CCRs and aluminum. Second, the C_R value of Ajisai shows a large semi-annual pattern. This semi-annual variation is caused by the periodic variation in cross-sectional area of Ajisai due to the attached fitting ring and the low reflectivity of the surface material in the polar regions. This variation of the cross-sectional area amounts to about 1% and has not been considered in the past.

We also point out that there is a clear difference of C_R^{POD} between LAGEOS-1 and LAGEOS-2, which are thought to be identically manufactured satellites. Although the cause has not been clarified, one of the possible reasons is the subtle difference of the surface finish.

The state-of-the-art SLR observations combined with highly sophisticated POD software enable us to provide an improved surface force model of the solar radiation pressure. Conclusively, it is important to investigate the optical properties of a satellite before launch.

Acknowledgements

The authors would like to thank Dr. A. Sengoku and Dr. H. Hashimoto for their useful comments. We also thank all developers of the c5++ software in Japan and in Sweden. Finally, we gratefully acknowledge the International Laser Ranging Service (ILRS) for obtaining and archiving the SLR observation data.

References

Altamimi, Z., Rebischung, P., Métivier, L., Collilieux, X., 2016. ITRF2014: a new release of the international terrestrial reference frame modeling nonlinear station motions. J. Geophys. Res.: Solid Earth 121 (8), 6109–6131.

Appleby, G., Rodríguez, J., Altamimi, Z., 2016. Assessment of the accuracy of global geodetic satellite laser ranging observations and estimated impact on ITRF scale: estimation of systematic errors in LAGEOS observations 1993-2014. J. Geodesy 90 (12), 1371–1388.

Bruinsma, S., 2015. The DTM-2013 thermosphere model. J. Space Weather Space Climate 5, A1.

Folkner, W.M., 2010, JPL Interoffice Memorandum, 1, 343.

Fitzmaurice, M.W., Minott, P.O., Abshire, J.B., Rowe, H.E., 1977. Prelaunch Testing of the Laser Geodynamic Satellite (LAGEOS), NASA Technical Paper, (1062).

Hashimoto, H., Private communications.

Haynes, W.M., Lide, D.R., Bruno, T.J. (Eds.), 2014. CRC Handbook of Chemistry and Physics, 95th ed. CRC Press.

Kopp, G., Lean, J.L., 2011. A new, lower value of total solar irradiance: evidence and climate significance. Geophys. Res. Lett. 38.

Kucharski, D., Otsubo, T., Kirchner, G., Koidl, F., 2010. Spin axis orientation of Ajisai determined from Graz 2 kHz SLR data. Adv. Space Res. 46 (3), 251–256.

Matsuo, K., Chao, B.F., Otsubo, T., Heki, K., 2013. Accelerated ice mass depletion revealed by low-degree gravity field from satellite laser ranging: greenland, 1991-2011. Geophys. Res. Lett. 40 (17), 4662–4667.

McCarthy, D.D. (Ed.), 1996. IERS Conventions (1996), IERS Technical Note, 21. <https://www.iers.org/IERS/EN/Publications/TechnicalNotes/tn21.html>.

Milani, A., Nobill, A.M., Farinella, P., 1987. Non-gravitational Perturbations and Satellite Geodesy. Adam Hilger Ltd., Accord, MA, USA.

Minott, P.O., Zagwodzki, T.W., Varghese, T., & Selden, M. 1993. Prelaunch Optical Characterization of the Laser Geodynamic Satellite (LAGEOS 2), NASA Technical Paper, (3400).

Montenbruck, O., Steigenberger, P., Darugna, F., 2017. Semi-analytical solar radiation pressure modeling for QZS-1 orbit-normal and yaw-steering attitude. Adv. Space Res. 59 (8), 2088–2100.

Noll, C., 2010. The crustal dynamics data information system: a resource to support scientific analysis using space geodesy. Adv. Space Res. 45 (12), 1421–1440.

Otsubo, T., Amagai, J., Kunimori, H., Elphick, M., 2000. Spin motion of the AJISAI satellite derived from spectral analysis of laser ranging data. IEEE Trans. Geosci. Remote Sens. 38 (3), 1417–1424.

Otsubo, T., Appleby, G.M., 2003. System-dependent center-of-mass correction for spherical geodetic satellites. J. Geophys. Res.: Solid Earth 108 (B4), 2156–2202.

Pavlis, N.K., Holmes, S.A., Kenyon, S.C., Factor, J.K., 2012. The development and evaluation of the Earth Gravitational Model 2008 (EGM2008). J. Geophys. Res.: Solid Earth 117, B04406.

Pearlman, M.R., Degnan, J.J., Bosworth, J.M., 2002. The international laser ranging service. Adv. Space Res. 30 (2), 135–143. https://doi.org/10.1016/S0273-1177(02)00277-6.

Petit, G., Luzum, B., (Eds.) 2010. IERS Conventions (2010), IERS Technical Note, 36. <https://www.iers.org/IERS/EN/Publications/TechnicalNotes/tn36.html>.

Sasaki, M., Hashimoto, H., 1987. Launch and observation program of the experimental geodetic satellite of Japan. IEEE Trans. Geosci. Remote Sens. 25 (5), 526–533.

Scharroo, R., Wakker, K.F., Ambrosius, B.A.C., Noomen, R., 1991. On the along-track acceleration of the LAGEOS satellite. J. Geophys. Res. 96 (90), 729–740.

Sengoku, A., Cheng, M.K., Schutz, B.E., 1995. Anisotropic reflection effect on satellite, Ajisai. J. Geodesy 70 (3), 140–145.

Siry, J., 1975. The LAGEOS system, NASA Technical Paper.

Sośnica, K., Jäggi, A., Meyer, U., Thaller, D., Beutler, G., Arnold, D., Dach, R., 2015a. Time variable Earth's gravity field from SLR satellites. J. Geodesy 89 (10), 945–960.

Sośnica, K., Jäggi, A., Thaller, D., Beutler, G., Dach, R., 2014. Contribution of Starlette, Stella, and AJISAI to the SLR-derived global reference frame. J. Geodesy 88, 789–804.

Sośnica, K., Thaller, D., Dach, R., Steigenberger, P., Beutler, G., Arnold, D., Jäggi, A., 2015b. Satellite laser ranging to GPS and GLONASS. J. Geodesy 89, 725–743.

Sośnica, K., Thaller, D., Jäggi, A., Dach, R., Beutler, G., 2012. Sensitivity of Lageos orbits to global gravity field models. Artif. Satellites 47 (2), 47–65.

Steigenberger, P., Montenbruck, O., Hugentobler, U., 2015. GIOVE-B solar radiation pressure modeling for precise orbit determination. Adv. Space Res. 55 (5), 1422–1431.

Tan, B., Yuan, Y., Zhang, B., Ze Hsu, H., Ou, J., 2016. A new analytical solar radiation pressure model for current BeiDou satellites: IGGBSPM. Sci. Rep. 6, 32967.

Ziebart, M., Dare, P., 2001. Analytical solar radiation pressure modelling for GLONASS using a pixel array. J. Geodesy 75 (11), 587–599.